ISIJ International, Vol. 39 (1999), No. 11, pp. 1140–1149

Application of the Sulphide Capacity Concept on High-basicity Ladle Slags Used in Bearing-Steel Production

Margareta A. T. ANDERSSON, Pär G. JÖNSSON and Mselly M. NZOTTA

Department of Metallurgy, Royal Institute of Technology, S-100 44 Stockholm, Sweden.

(Received on June 3, 1999; accepted in final form on July 26, 1999)

A rigorous evaluation of the usefulness of some existing models for prediction of sulphide capacity and sulphur distribution for industrial slags at Ovako Steel AB has been carried out. The results show that the best agreement between calculated and analysed sulphur distributions is obtained by calculating the alumina activity in the slag from an expression suggested by Ohta and Suito,[26] then using these data to calculate the oxygen activity in the molten steel, and finally by applying the KTH model[4–6] to calculate the sulphide capacity and sulphur distribution. Therefore, the conclusion is that the KTH model[4–6] is a useful tool for predictions of sulphur distributions for ladle slags.

KEY WORDS: desulphurisation; sulphide capacity; sulphur distribution; ladle treatment; slag; vacuum degassing; oxygen activity.

1. Introduction

In the production of ball-bearing steel grades it is of great importance to keep the level of oxide non-metallic inclusions as low as possible, especially inclusions larger than 15 μm, since they may initiate cracks.[1] The role of sulphur is somewhat more complex. Sulphur will form sulphides in the material during solidification and in some ball-bearing applications a certain sulphur level is positive, because the precipitated sulphides will be favourable for the cutting operation. On the other hand, sulphides will create anisotropy in the material during working, since they are easily deformed. In cases where there is a high load in different directions, the sulphides could act as crack initiators, similar to large calcium aluminates.[2] Since the average total oxygen content (amount of oxide inclusions) in bearing steel has been significantly reduced from 11 ppm in 1985 to 5 ppm in 1998 at Ovako Steel,[3] the importance of sulphides, acting as possible crack initiators, has increased. As a consequence, it is even more important to control the sulphur level.

The present paper is focused on the thermodynamic aspect of sulphur refining during vacuum degassing of ball-bearing steel grades. A model developed at the Department of Metallurgy,[4–6] KTH has been used to evaluate the sulphide capacity of the ladle slags. An initial attempt to use this model to evaluate the sulphide capacity for slags in production of medium-carbon steel grades of lower slag basicity has recently been carried out.[7] However, in the present paper a more rigorous evaluation of the application of the model to an industrial case is presented. Furthermore, these predictions of the sulphur-absorbing capacity of the slags are compared to predictions made by the optical basicity concept. Emphasis is also placed on the slag sampling reliability and the change in slag composition during ladle treatment.

In the first part of the paper, the theories behind sulphide capacity and sulphur distribution are outlined. Thereafter, the plant trials at Ovako Steel using high-basicity slags are described. Finally, the results of the evaluation of the plant trials with respect to reliability of slag sampling, change in top slag composition, oxygen activity, sulphide capacity, and sulphur distribution are discussed.

2. Theoretical Background

2.1. The Sulphide Capacity Concept

When discussing sulphur refining during steelmaking there are two important exchange reactions that should be considered[8]

$$\tfrac{1}{2}S_2(g)+(O^{2-})_{slag}=\tfrac{1}{2}O_2(g)+(S^{2-})_{slag} \quad \text{.....(1)}$$

$$\underline{S}_{metal}+(O^{2-})_{slag}=\underline{O}_{metal}+(S^{2-})_{slag} \quad \text{.....(2)}$$

Reaction (1) describes the favourable equilibrium between the slag phase and the gas phase with respect to sulphur and oxygen at partial pressures of oxygen less than 10^{-6} atm, which generally is fulfilled during ladle treatment of molten steel. Reaction (2) describes the corresponding equilibrium between the slag phase and the metal phase.

The equilibrium constant for reaction (1) could be expressed as

$$K_1=\frac{a_{S^{2-}}}{a_{O^{2-}}}\cdot\sqrt{\frac{p_{O_2}}{p_{S_2}}}=\frac{f_{S^{2-}}\cdot(\%S)_{slag}}{a_{O^{2-}}}\cdot\sqrt{\frac{p_{O_2}}{p_{S_2}}} \quad \text{.....(3)}$$

where $a_{S^{2-}}$ and $a_{O^{2-}}$ are the activities of sulphur and

oxygen in the slag phase, p_{S_2} and p_{O_2} are the partial pressures of S_2 (g) and O_2 (g), $f_{S^{2-}}$ is the activity coefficient of sulphur in the slag phase and $(\%S)_{slag}$ is the sulphur content in the slag in wt%.

The sulphide capacity C_S was defined by Richardson and Fincham[9] using Eq. (3)

$$C_S = \frac{K_1 \cdot a_{O^{2-}}}{f_{S^{2-}}} = (\%S)_{slag} \cdot \sqrt{\frac{p_{O_2}}{p_{S_2}}} \quad \text{.....(4)}$$

where K_1 is the equilibrium constant for Eq. (1). The sulphide capacity is a property of the slag, which is dependent only on the temperature and the slag composition. It describes the potential ability of an arbitrary homogeneous molten slag to remove sulphur and it could be used to compare the desulphurisation characteristics of different slags.

The sulphide capacity has been shown to correlate well with the basicity of the slag.[10] In the present paper the basicity in its most simple form is defined as the ratio between the basic oxide CaO and the acid oxide SiO_2 in weight percents. There are several more complex expressions of basicity that were found in the literature.[11]

2.2. Sulphide Capacity Models

Several models have been developed in order to estimate how the sulphide capacity of a slag varies with composition and temperature. An empirical expression was developed by Sosinsky and Sommerville,[12] where the composition dependence was defined by the concept of optical basicity. Later, Young *et al.*[13] modified this expression. The concept of using the optical basicity to predict the sulphide capacity has a great advantage because the method of calculation is not complicated. As a consequence, this approach has been rather attractive and practical for many metallurgists.

The optical basicity was originally introduced by Duffy and Ingram[14] and is a measure of the electron donor power of the oxides. Suggested values of the optical basicity for different oxides together with necessary equations for calculation of the optical basicity of a multicomponent slag are given in the literature.[12,13]

Sosinsky and Sommerville[12] derived a correlation between the optical basicity, the temperature and the sulphide capacity of an oxide slag at temperatures between 1 400 and 1 700°C

$$\log C_S = \left(\frac{22\,690 - 54\,640 \cdot \Lambda}{T}\right) + 43.6 \cdot \Lambda - 25.2 \quad \text{..(5)}$$

where T is the temperature and Λ is the optical basicity for the multicomponent slag. Later, Young *et al.*[13] found that this expression exhibited an increasing deviation between the measured and the calculated data at higher values of the sulphide capacity. They modified the expression and suggested the following relationship (used in the present paper)

$\Lambda < 0.8$:

$$\log C_S = -13.913 + 42.84 \cdot \Lambda - 23.82 \cdot \Lambda^2 - \left(\frac{11710}{T}\right) - 0.02223 \cdot (\%SiO_2) - 0.02275 \cdot (\%Al_2O_3) \quad \text{.....(6)}$$

where the contents of SiO_2 and Al_2O_3 are given in wt%.

Another sulphide capacity model was derived by Reddy and Blander,[15,16] who employed a Flory model to describe the sulphide capacities of binary slags. Pelton *et al.*[17] extended this model to multicomponent slags. To use the multicomponent model, it is necessary to have access to a database (F*A*C*T), which has not been available to the authors. Thus, no comparisons have been made in the present work.

Gaye *et al.*[18,19] have developed a statistical thermodynamic cell model, known as the IRSID slag model, which is able to predict the chemistry of multicomponent liquid slags important in steelmaking. The model was originally developed for oxide slags, which could be considered as single anionic, and was applied on the slag system Al_2O_3–CaO–Fe_2O_3–FeO–MgO–MnO–SiO_2. The slag structure was described according to Frohberg and Kapoor's model.[20] The formalism of the model was later extended to polyanionic slags, which could be applied to sulphur and fluorine bearing systems.[21] The IRSID slag model is used in the present work as one possible tool for estimation of oxide activities in the molten slag phase. The calculation of sulphur distributions between slag and metal when applying the IRSID slag model[18,19] were considered to be outside the scope of the present paper, but is currently being done.

A model for calculation of the sulphide capacity for multicomponent slags at different temperatures has also been developed at the Department of Metallurgy, KTH.[4–6] The model enables the prediction of the sulphide capacities of multicomponent slags from the data of lower-order systems. In earlier studies carried out within the Department of Metallurgy experimental data of sulphide capacities from laboratory experiments have been used to verify model predictions of ternary,[4] quarternary,[5] quinary[5] and six-component[6] slag systems.

The expression of sulphide capacity from Eq. (4) is represented with the following relationships

$$K_1 = \exp\left(-\frac{\Delta G^\circ}{R \cdot T}\right) \quad \text{.....(7)}$$

and

$$\frac{a_{O^{2-}}}{f_{S^{2-}}} = \exp\left(-\frac{\sum (X_i \cdot \xi_i) + \xi_{mix}}{R \cdot T}\right) \quad \text{.....(8)}$$

where, in Eq. (7), ΔG° is the Gibbs free energy of reaction (1) and R is the gas constant. In Eq. (8), i stands for component i and X_i is the molar fraction of component i in the multicomponent system. The term ξ_i is expressed as a linear function of the temperature for each component in the slag in the absence of interaction between different species. ξ_{mix} represents the mutual interaction (binary and ternary) between different species in the slag. ξ_{mix} is dependent on slag composition and temperature. In order to express the mixing, the liquid slag is described by a modified Temkin[22] approach, which considers the mixing of cations and anions within each of their subgroupings. More details regarding the equations and the assessed parameters necessary for

the calculation have been presented elsewhere.[4-6]

In the model, pure liquid FeO is chosen as the standard, for which the ratio $a_{O^{2-}}/f_{S^{2-}}$ is taken as unity. ΔG° is calculated from sulphide capacity measurements of pure liquid FeO as

$$\Delta G^\circ = 118\,535 - 58.815 \cdot T \quad \text{(J/mol)} \quad \text{.....(9)}$$

2.3. Calculation of Sulphur Distribution

In order to relate the sulphide capacity to the equilibrium sulphur distribution between the slag and metal phases, reactions (1) and (2) are combined to

$$\underline{S}_{metal} + \tfrac{1}{2}O_2(g) = \underline{O}_{metal} + \tfrac{1}{2}S_2(g) \quad \text{.....(10)}$$

The equilibrium constant K_{10} is expressed as[23]

$$\log K_{10} = -\frac{935}{T} + 1.375 \quad \text{.....(11)}$$

The equilibrium constant K_{10} can also be written as

$$K_{10} = \frac{a_O}{a_S} \cdot \sqrt{\frac{p_{S_2}}{p_{O_2}}} = \frac{(\%S)_{slag}}{[\%S]_{metal}} \cdot \frac{a_O}{f_S \cdot C_S} \quad \text{.....(12)}$$

where a_O and a_S are the activities of oxygen and sulphur in the metal phase, f_S is the activity coefficient for sulphur in the metal phase and $[\%S]_{metal}$ is the sulphur content in the metal phase.

By combining Eqs. (4), (11) and (12), the following expression for the equilibrium sulphur distribution L_S between the slag and metal phases is obtained[23]

$$\log L_S = \log \frac{(\%S)_{slag}}{[\%S]_{metal}} = -\frac{935}{T} + 1.375 + \log C_S + \log f_S - \log a_O \quad \text{...(13)}$$

In order to calculate the equilibrium sulphur distribution (L_S) between slag and steel in the present paper, Eq. (13) was used. The sulphide capacity was first calculated by using the model developed by the Department of Metallurgy, KTH.[4-6] For the purpose of comparison, the sulphide capacity was also calculated using both Sosinsky and Sommerville's[12] and Young's[13] relationships based on the optical basicity concept. The slag compositions used in the calculations were normalised to a four-component system (Al_2O_3–CaO–MgO–SiO_2), since the combined sum of these oxides was 97 wt% or more in all the analysed slag samples.

The activity coefficient in the steel bath was calculated by using Wagner's equation

$$\log f_j = \sum (e_j^i \cdot [\%i]) \quad \text{.....(14)}$$

where f_j is the activity coefficient for element j in the molten steel, i represents the dissolved elements in the molten steel and e_j^i is the interaction parameter for element j. The interaction parameters were in the present case taken from Engh.[24]

The oxygen activity in the steel bath, a_O, was calculated by assuming that the dissolved aluminium and oxygen in the steel bath and alumina in the top slag was in equilibrium according to the following reaction

$$2\underline{Al} + 3\underline{O} = Al_2O_3(s) \quad \text{.....(15)}$$

$$\Delta G^\circ = -1205\,115 + 386.714 \cdot T \quad \text{(J/mol)} \quad \text{.....(16)}$$

The data for the change of Gibbs free energy, Eq. (16), were taken from Hayes.[25] Solid alumina was chosen as the standard state. Therefore, the equilibrium constant, K_{15}, for Eq. (15) could be written as

$$K_{15} = \exp\left(\frac{-\Delta G^\circ}{R \cdot T}\right) = \frac{a_{Al_2O_3}}{a_{Al}^2 \cdot a_O^3} \quad \text{.....(17)}$$

where $a_{Al_2O_3}$ is the activity of alumina in the slag phase and a_{Al} is the activity of aluminium in the metal phase.

In order to calculate the oxygen activity (a_O) from the above equation, the activities of aluminium in the molten steel and alumina in the top slag need to be estimated.

The activity of aluminium in the molten steel could be expressed as

$$a_{Al} = f_{Al} \cdot [\%Al] \quad \text{.....(18)}$$

where f_{Al} is the activity coefficient of aluminium in the metal phase and [%Al] is the aluminium content by weight in the steel. The activity coefficient f_{Al} was calculated using Eq. (14).

The activity of alumina in the top slag was more difficult to estimate due to the lack of reliable experimental data in the Al_2O_3–CaO–MgO–SiO_2 system. There are different models that can be used to estimate the activity of oxide components in molten slags, such as the IRSID slag model,[18,19] which has been mentioned earlier. Also, in a recent publication, Ohta and Suito[26] presented empirical expressions for the activities of SiO_2 and Al_2O_3 at 1 600°C. In the present work both the empirical expression by Ohta and Suito[26] and the IRSID slag model[18,19] were used for estimation of the alumina activity.

Ohta and Suito[26] used a slag–metal equilibrium technique to determine the activity data.

A multiple regression analysis gave the following expression for the alumina activity in the slag

$$\log a_{Al_2O_3} = \frac{\{-0.275(\%CaO) + 0.167(\%MgO)\}}{(\%SiO_2)} + 0.033(\%Al_2O_3) - 1.560 \quad \text{.....(19)}$$

where the slag composition is given in wt%.

The composition range, where the expression by Ohta and Suito[26] is suggested to be employed, is for CaO: 10–60%, SiO_2: 10–50%, Al_2O_3: 0–50% and MgO: 0–30%. The slag compositions in the present paper were within this range, except for SiO_2, for which the content varied from about 6 to 13%. However, it was assumed that Eq. (19) could be extrapolated below 10% SiO_2 in order to get an estimation of the activity of Al_2O_3 for the studied slag system. The possible effects of this extrapolation on the equilibrium sulphur distribution will be discussed later in the paper. Furthermore, literature data[27] have indicated that there is almost no temperature dependence for the activity coefficient of alumina in slags. Therefore, it was assumed that the expression of Ohta and Suito[26] could be used in the present work, since the studied temperatures were close to 1 600°C.

The IRSID slag model[18,19] was also used for a comparative estimation of the alumina activity in the

Table 1. Interval of slag compositions from the plant trials at Ovako Steel.

Sampling	%MgO	%Al_2O_3	%SiO_2	%CaO	Σ Rest oxides
S1	7.3 - 10.0	25.3 - 29.1	5.7 - 9.4	51.0 - 58.2	1.1 – 3.0
S2	8.5 - 11.8	28.0 - 33.5	5.9 - 12.6	46.6 - 53.4	0.7 – 2.2
S3	8.5 - 11.3	28.3 - 33.6	5.8 - 12.7	46.7 – 53.8	0.5 – 2.6

slag phase. In the present work, the thermodynamic computer program THERMOCALC (version M), developed at KTH,[28] has been used, since it includes the IRSID slag model. Equilibrium was assumed between three phases in the calculation: liquid iron, liquid slag and solid MgO. The last condition was due to the fact that the slag in the ladle was always in contact with a MgO refractory lining. Therefore, it was assumed that the slag was MgO saturated. The input slag compositions for the calculation were the Al_2O_3, CaO and SiO_2 contents in each slag sample, indicated in **Table 1**. The temperatures are given in Table 3. Using this information, the activity of alumina at the point of MgO saturation in the liquid slag was calculated. For this calculation a small amount of iron oxide was always present in the liquid slag phase.

3. Plant Trials

3.1. Process Description

Ovako Steel has a scrap-based steel plant located in Hofors, Sweden. The scrap is melted in a 100 t oval bottom-tapped (OBT) electric-arc furnace. The raw steel is modified with respect to the desired phosphorus, carbon and temperature levels before it is tapped into a ladle. The ladle refractory is carbon-bound magnesite and predeoxidation is done during the tapping. The ladle is then transported to an ASEA-SKF ladle furnace (LF) station, where careful deslagging of the furnace slag is done before the secondary refining operation starts. The secondary refining operation is carried out in three main steps. In the first step, a synthetic slag mixture is added along with alloys and aluminium. The composition of the synthetic slag mixture used in these trials is given in Table 1. Graphite electrodes are used for melting the synthetic slag formers and to compensate for heat loss. Induction stirring is used for homogenisation of temperature and alloying additions. In the second step, the steel is vacuum degassed in order to remove hydrogen and sulphur. Inert gas stirring (argon) through two porous plugs gives rise to a large surface area between the argon bubbles and liquid steel which is beneficial for hydrogen removal. The intense stirring also results in mixing of the molten steel and the slag which enhances the removal of sulphur. In the third step, induction stirring is used to promote the separation of inclusions from the molten steel to the top slag. Only mild induction stirring is utilised in order to minimise reactions between steel and slag as well as reoxidation from the atmosphere. During this final step the steel and slag are also heated with electrodes to obtain the correct casting temperature. If necessary, a final adjustment of the steel composition by alloy additions is also done. After the ladle treatment is finished the steel is cast into 4.2 t ingots by uphill teeming.

3.2. Experimental Procedure

In the present paper, eight heats of a high-carbon chromium bearing steel grade of 1 wt% C and about 1.4 wt% Cr were studied. In all trials, a commercial synthetic slag mixture was added which resulted in a top slag composition of about 25–29 wt% Al_2O_3, 51–58 wt% CaO, 7–10 wt% MgO and 6–9 wt% SiO_2 before vacuum degassing. The total pressure during the degassing operation was 1–2 torr for all the heats.

Slag and steel samples were collected during ladle treatment corresponding to the three main steps of the secondary refining operation:

- The first sampling (S1) was done at the end of the initial heating and alloying period.
- The second sampling (S2) was done just after the vacuum degassing operation.
- The third sampling (S3) was done at the end of the final stirring and heating period.

The temperature of the molten steel was measured with each sampling. Both the temperature measurements and the steel samples were taken using the automatic sampling equipment at the LF station. Slag samples were collected manually with a slag spoon.

For most heats only one slag sample was taken on each sampling occasion, but for two heats three slag samples were collected at the S1 and S2 samplings. For these two heats (heat E and F), three different sampling positions in the top slag were chosen. The composition of each sample was analysed separately. The purpose was to study the degree of homogenisation of the slag before and after the vacuum degassing operation and to evaluate the reliability of data obtained from the sampling procedure.

3.3. Analysis Procedure

Almost the whole amount of each collected slag sample was well ground to get an evenly mixed powder, from which a representative portion could be taken for analysis. Each ground slag sample was examined for metallic iron, which was carefully removed with a magnet. The slag samples were then analysed with an X-ray fluorescence method (Siemens SRS 303) to determine their oxide compositions. The relative analysis accuracy was ±3%. The slag samples were also separately analysed for sulphur by using a melting and combustion method (Rosemount CSA 5003). The relative analysis accuracy for this was also ±3%.

The steel samples were analysed by Optical Emission Spectroscopy (Bausch & Lomb, ARL OES 3560). The relative analysis accuracy for the elements Al, Cr, Mn and Si was within ±5%. Carbon and sulphur in the steel samples were analysed using the fusing method (LECO CS-244). For carbon and sulphur the relative analysis accuracy was ±0.7% and ±5.4%, respectively.

4. Results and Discussion

The results of the analysed slag and steel samples together with the measured steel temperatures are shown in **Tables** 1, **2** and **3**. The oxide components of the slag were normalised to 100%. The sulphur contents of the slag samples are given separately. In all the analysed slag samples, the sum of Al_2O_3, SiO_2, MgO and CaO was 97% or more and in many cases more than 98%.

4.1. Reliability of Slag Sampling

The reliability of slag sampling was studied in two ways. First, multiple samples from one sampling occasion were evaluated. Second, the differences between the sulphur contents in the slag after vacuum treatment (S2) and after final heating and stirring (S3) were evaluated.

The accuracy of the multiple sampling before (S1) and after (S2) vacuum degassing is shown in **Table 4** for heats E and F. The results are based on three separate slag samples. Besides the calculated average value and its standard deviation, the relative standard deviation is shown. The latter was calculated as the standard deviation divided by the average value. Also, note that the oxide composition has been normalised to 100% and based on four components: MgO, Al_2O_3, SiO_2, and CaO.

The oxide compositions in Table 4 were quite consistent between the different samples both for the samples taken before and after vacuum treatment. The largest relative standard deviation for an individual oxide component was 5.8%. However, in most cases the relative standard deviations are within the relative accuracy of analysis (±3%).

Also, the sulphide composition before vacuum treatment was very consistent. The relative standard deviation for heats E and F is 0% and 1.4%, respectively. This was probably due to the fact that the desulphurisation had not begun yet. Also, the determined sulphur content probably derived both from remaining EAF furnace slag and added synthetic slag.

Sulphur data from the multiple sampling after vacuum degassing (S2) deviated more than for the S1 analysis. For heat E, the average sulphur content after vacuum degassing was 2.9% with a standard deviation of 0.46%. For heat F, the corresponding value was 2.2% with a standard deviation of 0.23%. Furthermore, the relative standard deviation was as high as 15.9% and 10.4% for heats E and F, respectively. This should be compared to the relative accuracy of the laboratory analysis procedure, which was maximum ±3% of the analysis data. Even though multiple sampling was only done for two heats, it was possible to conclude that the sampling method could significantly affect determined sulphur

Table 2. Sulphur contents in steel and slag samples.

Heat	$[\%S]_{steel}$	$(\%S)_{slag}$
A-1	0.026	0.59
A-2	0.009	2.0
A-3	0.009	2.1
B-1	0.027	0.81
B-2	0.004	3.2
B-3	0.004	3.0
C-1	0.022	0.35
C-2	0.005	2.4
C-3	0.006	2.3
D-1	0.034	0.48
D-2	0.007	2.5
D-3	0.008	2.5
E-1	0.034	0.47
E-2	0.008	2.9
E-3	0.007	3.3
F-1	0.024	0.44
F-2	0.007	2.2
F-3	0.006	2.2
G-1	0.025	0.44
G-2	0.009	2.0
G-3	0.008	2.1
H-1	0.029	0.62
H-2	0.010	2.4
H-3	0.009	2.1

Table 3. Compositions of alloying elements and temperatures of the steel from the plant trials at Ovako Steel. Only the major elements are included. The steel grade contained 1% C and 1.4% Cr.

Heat	%Si	%Mn	%Al	Temperature (°C)
A-1	0.23	0.28	0.033	1621
A-2	0.22	0.28	0.015	1536
A-3	0.22	0.28	0.024	1533
B-1	0.28	0.30	0.067	1575
B-2	0.28	0.29	0.033	1522
B-3	0.25	0.27	0.031	1532
C-1	0.24	0.27	0.066	1598
C-2	0.26	0.27	0.040	1508
C-3	0.25	0.27	0.031	1536
D-1	0.24	0.27	0.066	1578
D-2	0.26	0.28	0.032	1509
D-3	0.26	0.28	0.029	1534
E-1	0.29	0.28	0.060	1587
E-2	0.30	0.28	0.035	1534
E-3	0.30	0.28	0.035	1535
F-1	0.24	0.29	0.068	1621
F-2	0.26	0.29	0.035	1543
F-3	0.26	0.29	0.035	1537
G-1	0.10	0.28	0.071	1606
G-2	0.10	0.28	0.036	1545
G-3	0.10	0.28	0.034	1534
H-1	0.26	0.28	0.060	1602
H-2	0.26	0.29	0.036	1537
H-3	0.26	0.28	0.034	1536

Table 4. Reliability of slag sampling, evaluated for heat E and F and at the sampling occasions before (E-1 and F-1) and after (E-2 and F-2) vacuum degassing. The average values of the analysed oxide content in the slags are given in the table together with the standard deviations (within parantheses) and the relative standard deviations (%). The oxide components are normalised to 100%. The sulphur contents in the slag analysed using a separate fusing method are also given in the table.

Heat	%MgO	$\%Al_2O_3$	$\%SiO_2$	%CaO	%S
E-1: Average (±Std)	8.0 (±0.23)	27.2 (±1.16)	6.2 (±0.06)	58.8 (±1.04)	0.47 (±0)
E-1: Relative Std (%)	2.9	4.3	1.0	1.8	0
E-2: Average (±Std)	8.9 (±0.12)	33.3 (±0.06)	6.2 (±0.06)	51.6 (±0.10)	2.9 (±0.46)
E-2 Relative Std (%)	1.3	0.2	1.0	0.2	15.9
F-1: Average (±Std)	9.6 (±0.10)	28.9 (±0)	7.9 (±0.10)	53.6 (±0)	0.44 (±0.006)
F-1: Relative Std (%)	1.0	0	1.3	0	1.4
F-2: Average (±Std)	12.0 (±0.70)	33.7 (±0.17)	7.0 (±0.06)	47.4 (±0.49)	2.2 (±0.23)
F-2: Relative Std (%)	5.8	0.5	0.9	1.0	10.4

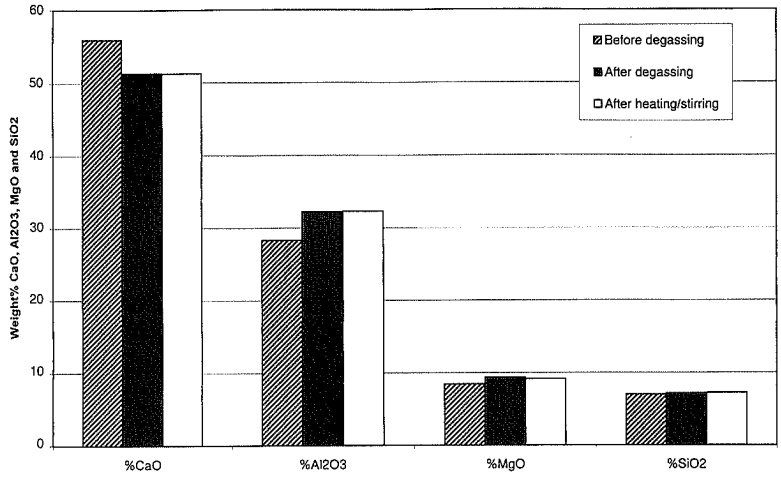

Fig. 1. Variation of the average top slag composition during ladle treatment.

contents in the slag after vacuum degassing. These results may also indicate that the slag was not completely homogeneous with respect to sulphur content after vacuum treatment.

Another way to evaluate the reliability of the sampling method was to compare the sulphur contents in the slag after degassing (S2) and final stirring/heating (S3). It was reasonable to assume that the sulphur content in the slag should not change much between these two sampling occasions. This was due to the fact that mild induction stirring is used, which minimised mixing of slag and steel and thereby sulphur refining. An evaluation of the eight heats (A–H) in Table 2 shows that the largest changes in sulphur content between S2 and S3 were 13.8% and −12.5%. However, for the majority of the heats the corresponding changes were within ±6.3%. The conclusion is that the change in sulphur content during degassing was less, or in extreme cases, of the same magnitude as the sampling accuracy.

To summarise, the oxide compositions were generally in good agreement between the different samples both for the samples taken before and after vacuum treatment. For the majority of the samples, the relative standard deviations were within the relative accuracy of analysis (±3%). Also, the sulphur compositions before vacuum treatment were very consistent, as was indicated from the value of the maximum relative standard deviation of 1.4%. For slag samples taken after vacuum treatment, however, the relative standard deviation in heats E and F was as high as 15.9% and 10.4%, respectively. When these values were compared with the sulphur analysis results from sampling at the end of ladle treatment, the large variation remained. Consequently, our conclusion is that the slag was not completely homogeneous with respect to sulphur after vacuum treatment. This may affect the sulphur distributions that were calculated from the analysed slag and steel sample data.

4.2. Slag Composition

The average composition of the top slag changed during the vacuum degassing, which is illustrated in **Fig. 1**. There was a clear increase in slag Al_2O_3 content, and at the same time a decrease in CaO. The increase of Al_2O_3 could be due to alumina inclusions, which were separated from the steel melt and assimilated in the slag. This statement was confirmed by results from an earlier study that showed that 44% of the inclusions originally found in the steel at the beginning of ladle treatment were removed from the molten steel during the vacuum degassing operation.[29] Another explanation could be that dissolved aluminium in the steel reacted with oxygen from reoxidation reactions and produced alumina, which ended up in the top slag. The corresponding decrease of CaO in Fig. 1 was probably only due to dilution of the slag. Also, in general, there was a small increase of MgO in the slag during vacuum degassing. Earlier studies have shown that this could be caused by refractory wear, which takes place at the low pressures existing during vacuum degassing.[30,31] Finally, it was also observerd that the SiO_2 content did not show any clear tendency to decrease nor increase during vacuum degassing.

As seen in Fig. 1, the composition of the top slag was more or less unchanged between the two last samplings, S2 and S3 (*i.e.* during the final heating and stirring period). This was expected since mild induction stirring is normally used in order to minimise reactions between steel and slag. The objective of the final LF treatment is to use the slag to protect the molten steel from the surrounding atmosphere and to assimilate the remaining non-metallic inclusions, which are being separated from the steel during the mild stirring. The supposed assimilation of inclusions could possibly explain a slight tendency of increase in Al_2O_3 content in the slag during the final stirring and heating period. This was confirmed by an earlier study that showed that a small amount of inclusions were separated from the melt during this part of the secondary treatment in the LF.[29] However, the change in alumina was within the accuracy of the analysis, so it was difficult to draw any clear conclusions.

To summarise, the Al_2O_3 content in the top slag significantly increased during the degassing operation. This could be due to separation of oxide inclusions and/or formation of Al_2O_3 as a reoxidation product. Another conclusion is that the MgO content increased slightly probably because of refractory wear. During the final heating and stirring period there was no significant change of the slag composition.

Table 5. Calculated Al_2O_3 activities in the slag phase and oxygen activities in the molten metal phase. The reference states for the activities of alumina in the slag phase and oxygen in the molten steel were solid Al_2O_3 and 1 wt% standard state, respectively.

Heat	Case 1:Activity of Al_2O_3 [25]	Case 1: Oxygen activity in molten steel [25]	Case 2: Activity of Al_2O_3 [27]	Case 2: Oxygen activity in molten steel [27]
A-1	$7.3\cdot10^{-3}$	$8.6\cdot10^{-5}$	$3.9\cdot10^{-4}$	$3.2\cdot10^{-5}$
A-2	$2.4\cdot10^{-2}$	$5.8\cdot10^{-5}$	$1.3\cdot10^{-3}$	$2.2\cdot10^{-5}$
A-3	$2.6\cdot10^{-2}$	$4.2\cdot10^{-5}$	$1.4\cdot10^{-3}$	$1.6\cdot10^{-5}$
B-1	$1.6\cdot10^{-3}$	$1.6\cdot10^{-5}$	$1.5\cdot10^{-4}$	$7.3\cdot10^{-6}$
B-2	$1.7\cdot10^{-3}$	$1.2\cdot10^{-5}$	$4.4\cdot10^{-4}$	$7.4\cdot10^{-6}$
B-3	$1.4\cdot10^{-3}$	$1.4\cdot10^{-5}$	$4.5\cdot10^{-4}$	$9.2\cdot10^{-6}$
C-1	$5.0\cdot10^{-3}$	$3.5\cdot10^{-5}$	$3.7\cdot10^{-4}$	$1.5\cdot10^{-5}$
C-2	$6.2\cdot10^{-3}$	$1.3\cdot10^{-5}$	$1.1\cdot10^{-3}$	$7.1\cdot10^{-6}$
C-3	$6.8\cdot10^{-3}$	$2.4\cdot10^{-5}$	$1.1\cdot10^{-3}$	$1.3\cdot10^{-5}$
D-1	$3.1\cdot10^{-3}$	$2.2\cdot10^{-5}$	$2.2\cdot10^{-4}$	$8.9\cdot10^{-6}$
D-2	$8.8\cdot10^{-3}$	$1.7\cdot10^{-5}$	$1.2\cdot10^{-3}$	$8.6\cdot10^{-6}$
D-3	$1.1\cdot10^{-2}$	$2.8\cdot10^{-5}$	$1.4\cdot10^{-3}$	$1.4\cdot10^{-5}$
E-1	$8\cdot10^{-4}$	$1.6\cdot10^{-5}$	$1.5\cdot10^{-4}$	$9.3\cdot10^{-6}$
E-2	$3.0\cdot10^{-3}$	$1.6\cdot10^{-5}$	$8.0\cdot10^{-4}$	$1.0\cdot10^{-5}$
E-3	$3.4\cdot10^{-3}$	$1.7\cdot10^{-5}$	$8.4\cdot10^{-4}$	$1.1\cdot10^{-5}$
F-1	$5.4\cdot10^{-3}$	$4.7\cdot10^{-5}$	$5.0\cdot10^{-4}$	$2.1\cdot10^{-5}$
F-2	$9.3\cdot10^{-3}$	$2.7\cdot10^{-5}$	$1.4\cdot10^{-3}$	$1.4\cdot10^{-5}$
F-3	$9.9\cdot10^{-3}$	$2.5\cdot10^{-5}$	$1.5\cdot10^{-3}$	$1.3\cdot10^{-5}$
G-1	$9\cdot10^{-4}$	$2.0\cdot10^{-5}$	$2.6\cdot10^{-4}$	$1.3\cdot10^{-5}$
G-2	$8.4\cdot10^{-3}$	$2.6\cdot10^{-5}$	$1.1\cdot10^{-3}$	$1.4\cdot10^{-5}$
G-3	$9.1\cdot10^{-3}$	$2.4\cdot10^{-5}$	$1.2\cdot10^{-3}$	$1.2\cdot10^{-5}$
H-1	$8.9\cdot10^{-3}$	$4.5\cdot10^{-5}$	$7.2\cdot10^{-4}$	$2.0\cdot10^{-5}$
H-2	$1.3\cdot10^{-2}$	$2.7\cdot10^{-5}$	$1.2\cdot10^{-3}$	$1.2\cdot10^{-5}$
H-3	$1.4\cdot10^{-2}$	$2.8\cdot10^{-5}$	$1.2\cdot10^{-3}$	$1.2\cdot10^{-5}$

4.3. Oxygen Activity

The estimated activities of Al_2O_3 according to Ohta and Suito's expression[26] (case 1) and the IRSID slag model[18,19] (case 2) are shown in **Table 5** together with the calculated oxygen activities. When Ohta and Suito's expression[26] was applied to the plant trial data, the top slag compositions for all heats were normalised to the Al_2O_3–CaO–MgO–SiO_2 four component system, since the sum of these oxides always was 97 wt% or more (see Table 1). There could be some error in the estimated activities of alumina in case 1, since the SiO_2 contents determined in the present work were primarily between 5.8 –12.7%, but Eq. (19) is only valid for a SiO_2 content of 10 to 50 wt%. All the other oxide components were within the limits given in the reference.[26]

The calculated oxygen activities were in general well below 10^{-4} (wt%) and sometimes even lower than 10^{-5}. The oxygen activities calculated in case 1 were about twice as high compared to the calculated data in case 2. As a comparison, oxygen sensor measurements carried out after vacuum degassing[32] have shown that the oxygen activity is between 0.76×10^{-4} to 1.2×10^{-4}. However, it is very difficult to measure the oxygen activity in molten steel with great accuracy at levels as low as 10^{-4} or below. In such cases the measured oxygen activity will always be higher than the real value due to electronic conduction in the electrolyte.[33,34] The measured oxygen activity should then be used with precaution. Thus, it was practically impossible in the present case to establish the actual oxygen activity in the molten steel by oxygen sensor measurements.

To summarise, the calculated oxygen activities in case 1 using Ohta and Suito's expression[26] were closer to the measured activities compared to case 2 (IRSID slag model). Furthermore, the calculated activities were lower than measured levels,[32] which would be expected at these low oxygen activity values.[33,34]

4.4. Sulphide Capacity

The sulphide capacities were calculated for all heats, using both the KTH model[4–6] and the concept of optical basicity.[12,13] When the optical basicity concept was used, the sulphide capacity was calculated both by using Sosinsky and Sommerville's Eq. (5)[12] and also the expression derived by Young *et al.*[13] The calculated values of the optical basicity Λ for the present slag compositions were in all cases less than 0.8. Thus, Eq. (6) was valid and could be used when calculating the sulphide capacity according to Young *et al.*[13] The results of the different calculated sulphide capacities are shown in **Table 6**. It was found that the optical basicity concept rendered larger values compared to the KTH model. The difference between the models increased with an increase in the slag basicity, which is seen in **Fig. 2**. It was not possible to make direct measurements of the sulphide capacity from the slag samples from the plant trials. Consequently it was difficult to decide only from Fig. 2 which one of the sulphide capacity models would be most applicable to sulphur refining. The sulphur distribution between the slag and metal was on the other hand, easy to measure and the evaluation of the models in the present paper was therefore based on these results. The effect of the difference between the sulphide capacity models on calculated sulphur distributions and the agreement with the experimentally determined values are discussed in the following section.

4.5. Sulphur Distribution

The equilibrium sulphur distributions according to Eq. (13) were calculated for all heats, using both the KTH model[4–6] and the concept of optical basicity[12,13] together with the oxygen activities from case 1 in Table 5. The equilibrium sulphur distribution from the KTH model[4–6] was also calculated using the oxygen activity values obtained in case 2. The results are shown in Table 6. The calculated equilibrium sulphur distribution values from the KTH-model and case 1 in Table 6 are also plotted in Fig. 3 against the sulphur distribution based on slag and steel sample analysis results. It was obvious that the slag and steel were not in equilibrium before the degassing operation took place, since the equilibrium L_S were larger than the determined sulphur distributions. Also, after vacuum degassing, the calculated L_S values decreased in almost all cases, while the analysis sulphur distribution values increased, which resulted in a remarkably good agreement between the two data sets. Furthermore, agreement was still very good after the final stirring and heating period.

There are two possible reasons for the decrease in calculated L_S values during the vacuum degassing treatment. First, the temperature decreased significantly during degassing, which lowered the sulphide capacity of the slag. Second, the slag composition changed towards decreased sulphide capacity values due to a decrease in CaO and an increase in Al_2O_3. This means that the best thermodynamic conditions for the refining of sulphur were in the beginning of the vacuum degassing operation. Furthermore, the kinetic conditions were also

Table 6. Calculated equilibrium sulphide capacities and sulphur distributions. *) Oxygen activities by using Eq. (19) from Ohta and Suito,[25] case 1 in Table 5. **) Oxygen activities by using the IRSID slag model and THERMOCALC,[27] case 2 in Table 5.

Heat	KTH model [4-6]			Optical basicity Sosinsky and Sommerville [12]		Optical basicity Young et al [13]	
	C_S	L_S *)	L_S **)	C_S	L_S *)	C_S	L_S *)
A-1	$3.32\cdot10^{-3}$	305.1	810.7	$1.63\cdot10^{-2}$	1500.3	$8.58\cdot10^{-3}$	786.6
A-2	$9.35\cdot10^{-4}$	147.5	390.3	$2.50\cdot10^{-3}$	394.6	$2.37\cdot10^{-3}$	374.1
A-3	$8.59\cdot10^{-4}$	189.8	498.0	$2.28\cdot10^{-3}$	502.8	$2.20\cdot10^{-3}$	485.3
B-1	$3.57\cdot10^{-3}$	1907.3	4214.2	$1.52\cdot10^{-2}$	8127.7	$1.03\cdot10^{-2}$	5495.5
B-2	$1.53\cdot10^{-3}$	1207.1	1902.3	$4.82\cdot10^{-3}$	3804.5	$3.98\cdot10^{-3}$	3141.4
B-3	$1.68\cdot10^{-3}$	1149.9	1690.6	$5.59\cdot10^{-3}$	3828.6	$4.31\cdot10^{-3}$	2949.9
C-1	$2.78\cdot10^{-3}$	620.0	1474.1	$1.35\cdot10^{-2}$	3003.6	$7.74\cdot10^{-3}$	1726.5
C-2	$9.53\cdot10^{-4}$	680.9	1215.4	$2.45\cdot10^{-3}$	1752.8	$2.30\cdot10^{-3}$	1640.4
C-3	$1.15\cdot10^{-3}$	451.4	818.5	$3.52\cdot10^{-3}$	1380.4	$2.86\cdot10^{-3}$	1122.6
D-1	$2.80\cdot10^{-3}$	1069.2	2596.7	$1.36\cdot10^{-2}$	5187.3	$8.33\cdot10^{-3}$	3181.6
D-2	$7.75\cdot10^{-4}$	425.8	821.5	$2.32\cdot10^{-3}$	1273.6	$2.28\cdot10^{-3}$	1255.4
D-3	$9.27\cdot10^{-4}$	308.3	620.4	3.00·10-3	998.8	$2.62\cdot10^{-3}$	870.2
E-1	$4.02\cdot10^{-3}$	2131.8	3767.2	$2.04\cdot10^{-2}$	10827.4	$1.04\cdot10^{-2}$	5509.5
E-2	$1.35\cdot10^{-3}$	785.9	1227.1	$4.30\cdot10^{-3}$	2503.0	$3.41\cdot10^{-3}$	1986.5
E-3	$1.35\cdot10^{-3}$	747.1	1193.4	$4.21\cdot10^{-3}$	2327.1	$3.32\cdot10^{-3}$	1839.7
F-1	$2.74\cdot10^{-3}$	467.9	1036.8	$1.59\cdot10^{-2}$	2722.6	$8.40\cdot10^{-3}$	1433.9
F-2	$9.38\cdot10^{-4}$	324.5	610.2	$3.44\cdot10^{-3}$	1189.3	$2.90\cdot10^{-3}$	1002.1
F-3	$8.91\cdot10^{-4}$	327.6	613.8	$3.05\cdot10^{-3}$	1121.4	$2.62\cdot10^{-3}$	964.4
G-1	$3.72\cdot10^{-3}$	1553.2	2369.0	$2.07\cdot10^{-2}$	8637.3	$9.90\cdot10^{-3}$	4132.6
G-2	$1.14\cdot10^{-3}$	390.1	757.0	$3.88\cdot10^{-3}$	1327.8	$3.13\cdot10^{-3}$	1069.5
G-3	$1.02\cdot10^{-3}$	381.0	739.1	$3.18\cdot10^{-3}$	1189.3	$2.71\cdot10^{-3}$	1010.6
H-1	$1.96\cdot10^{-3}$	369.1	851.6	$9.86\cdot10^{-3}$	1855.9	$6.11\cdot10^{-3}$	1150.9
H-2	$1.02\cdot10^{-3}$	353.9	789.1	$3.21\cdot10^{-3}$	1114.7	$2.79\cdot10^{-3}$	967.1
H-3	$9.71\cdot10^{-4}$	323.2	723.2	$3.10\cdot10^{-3}$	1032.7	$2.73\cdot10^{-3}$	908.9

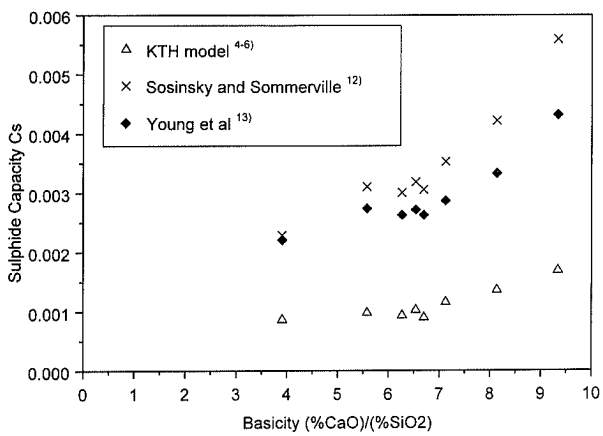

Fig. 2. Sulphide capacity values plotted as functions of the basicity.

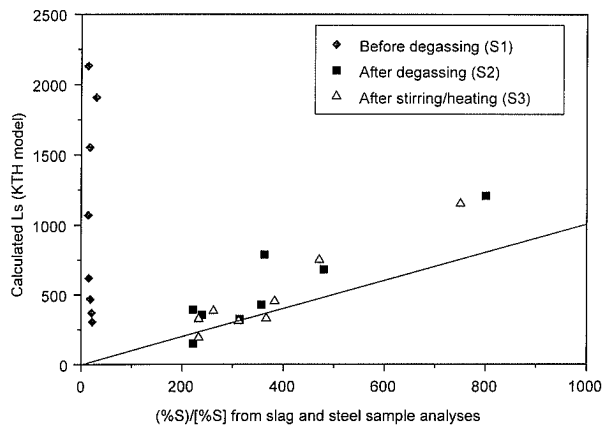

Fig. 3. Calculated L_S from the KTH model plotted as a function of the sample analysis sulphur distributions between slag and metal. The oxygen activities were calculated using Eqs. (14)–(19).

favourable due to large concentration gradients of sulphur (both in the slag and steel) and extensive mixing of steel and slag due to an intense argon bottom purging. Also, the sulphide capacity was high at the beginning of the vacuum treatment. As the top slag started to pick up sulphur, the concentration gradients became smaller, while the sulphide capacity decreased due to the above mentioned reasons. Thus, both the kinetic and the thermodynamic conditions became less and less favourable, until equilibrium or near equilibrium was reached.

The changes in the sulphur distribution ratio after the final heating and stirring period were relatively small for the majority of the heats, as is seen in Table 6. This was expected since the sulphur refining reaction was close to equilibrium after vacuum degassing. Furthermore, the conditions for sulphur refining were not very good when mild induction stirring was used, since it inhibited almost all mixing between steel and slag.

In order to compare the results using the KTH model to the predictions when the concept of optical basicity was used, the predicted sulphur distributions were plotted as a function of the analysis sulphur distribution data after the final stirring and heating period (S3) in **Fig. 4**. As seen, the predictions using the KTH model agreed well with the analysis sulphur distributions, but the predicted equilibrium values using the optical basicity concept were much higher.

One parameter that would affect the predicted sulphur distribution was the oxygen activity in the molten steel (see Eq. (13)). The effect of oxygen activity is illustrated in **Fig. 5** for predicted L_S values using the KTH model. The figure shows four data sets of calculated L_S values representing the end of the final stirring and heating period (S3). In two of the data sets, the oxygen activity is fixed to 10^{-5} and 10^{-4}. In the third and fourth data

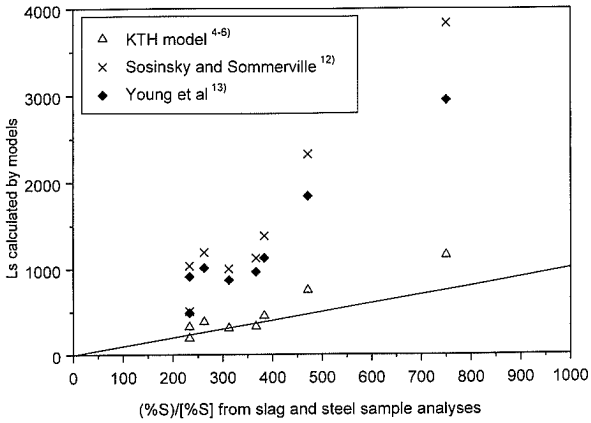

Fig. 4. Comparison of the KTH model and the optical basicity values at the end of ladle treatment. The oxygen activities were calculated using Eqs. (14)–(19).

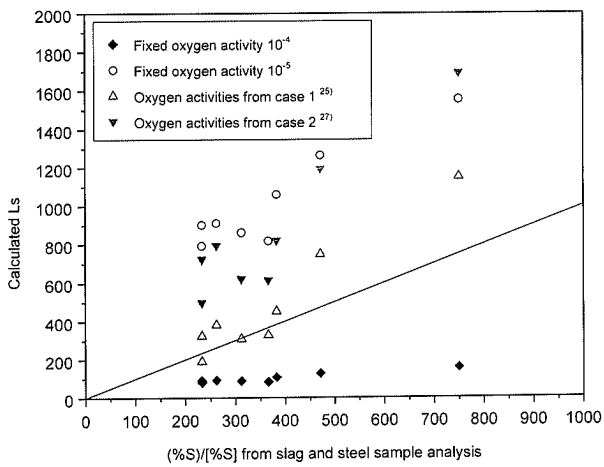

Fig. 5. Effect of the oxygen activity on the calculation of L_S. For estimation of the sulphide capacity the KTH model was used in all cases. The samples were taken at the end of ladle treatment (after final stirring/heating).

sets, the oxygen activities were taken from case 1 and case 2 in Table 5, respectively. As seen in Fig. 5, the equilibrium sulphur distributions were about twice as high when using the IRSID model (case 2) to estimate the oxygen activity compared to when using Ohta and Suito's[26] model (case 1) as a basis for calculating the oxygen activity. It can also be seen from Fig. 5 that in order for the calculated L_S values from the KTH model to agree with the analysis sulphur distribution values in the present case, the oxygen activity was estimated to be less than 10^{-4}.

Figure 6 shows the deviation (%) between the calculated sulphur distributions (using the KTH model together with case 1 in Table 5) and the analysis sulphur distributions as a function of basicity of slag samples taken after the final stirring and heating period (S3). The figure shows that there was a positive deviation when the basicity of the slag $(\%CaO)/(\%SiO_2)$ increased. This means that the model calculations predicted higher sulphur distributions at higher basicities compared to the plant data obtained.

One possible reason for the increased deviation between predicted and analysis sulphur distributions at higher basicities was that the use of Eq. (19) to calculate

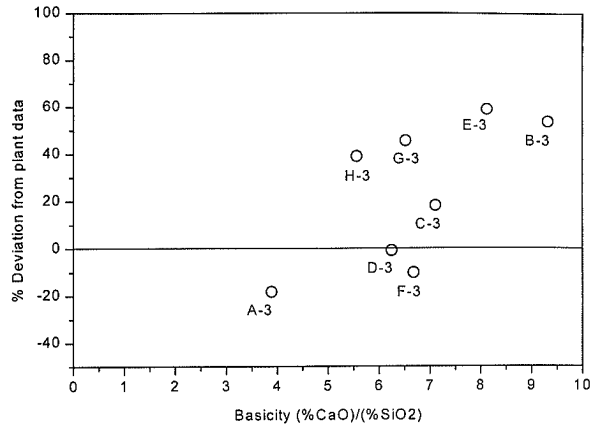

Fig. 6. Deviation (%) between calculated L_S (KTH model) and the analysis sulphur distribution values as a function of the basicity of the top slag. The samples were taken at the end of ladle treatment (after final stirring/heating).

the alumina activity might not be appropriate for those slags whose silica content was too far away from the specified lower limit of 10 wt%.[26] It was observed that the heats with the highest equilibrium sulphur distribution values also had the corresponding highest basicities and lowest silica contents (heats B and E). More specifically, the silica content in heat B, for example, was as low as 5.8 wt%. As a consequence of still using Eq. (19), the calculation of the alumina activity and subsequently the oxygen activity and its use in the KTH model may give too high values of the sulphur distribution ratio at higher basicities.

To summarise, the predicted sulphur distribution ratios did not agree with the experimentally determined values before vacuum degassing since the slag and steel were not in equilibrium. After the vacuum treatment the agreement was much improved since the thermodynamic and kinetic conditions for sulphur refining were very good during vacuum degassing, but the predicted values were still influenced by a number of conditions. First, it is shown in Fig. 4, that when using the KTH model, better agreement with the experimental values was obtained compared to when models based on the optical basicity concept were used. Second, it is shown in Fig. 4 that the way the oxygen activity was calculated influenced the predictions of L_s to a large degree. The best agreement between calculated and analysis sulphur distributions was obtained when calculating the alumina activities in the slag from Ohta and Suito's expression,[26] then using these data to calculate the oxygen activities in the molten steel, and finally applying the KTH model to calculate the sulphide capacities and sulphur distributions. Third, it is seen from Fig. 6 that the KTH model showed a tendency to predict a higher sulphur distribution ratio at higher basicities of the present slag compositions, especially when $(wt\%CaO)/(wt\%SiO_2)$ was greater than 6. For the slag samples with a high basicity, the silica content was lowest. For example, the silica contents was as low as 5.8 wt% in heat B, which was quite far from the lower limit of 10 wt% specified by Ohta and Suito[26] as the validity for Eq. (19) to calculate the alumina activity. As a consequence, it would necessary to modify Eq. (19) to be able to calculate

reliable data at lower silica contents if one should be interested in using high basicity slags ((wt%CaO)/(wt% SiO_2)>6). However, the authors' opinion is that for sulphur refining this should not be necessary. Currently, work is being conducted to determine optimum slag compositions for slag refining based on the use of the KTH model[4-6] and the expression of Ohta and Suito.[26]

5. Conclusions

The thermodynamic aspect of sulphur refining focusing on the sulphur distribution when producing bearing steel has been investigated. Several models and relationships have been used to predict the alumina activity in the slag,[18-20,26,28] oxygen activity in the steel, sulphide capacity of the slag,[4-6,12,13] and sulphur distribution.[23] The main overall conclusion is that the best agreement between calculated and analysis sulphur distributions was obtained when calculating the alumina activities in the slag from Ohta and Suito's expression,[26] then using these data to calculate the oxygen activities in the molten steel, and finally by applying the KTH model[4-6] to calculate the sulphide capacities and sulphur distributions. The more specific conclusions from this study are as follows:

- The slag was less homogeneous with respect to sulphur compared to oxides. The largest relative standard deviations of sulphur content and oxide content in the slag were 15.9% and 5.8%, respectively.
- During vacuum treatment, the Al_2O_3 content significantly increased due to separation of oxide inclusions and/or formation of Al_2O_3 as a reoxidation product and the MgO content increased slightly probably due to refractory wear. During the final heating and stirring period there was no significant change in slag composition.
- The calculated oxygen activities using Ohta and Suito's relationship[26] were closer to measured activities[32] compared to predictions from the IRSID model,[18-20,28] and in both cases the predictions were lower than measured values.
- Predictions of sulphide capacities using the expressions based on the optical basicity concept[12,13] rendered higher values compared to when the KTH model[4-6] was used.
- Predictions of the equilibrium sulphur distributions deviated more from the sample analysis distributions at higher basicities, while the alumina content in the slag was between 28.0 wt% to 33.6 wt%.

This study has shown that it is possible to use the KTH model[4-6] for prediction of sulphur distributions for specific plant slag compositions. Currently, work is being done to further evaluate the validity of the model predictions for different ladle slag compositions used in the industry.

Acknowledgements

The authors wish to acknowledge the support received from Ovako Steel AB throughout this work. Thanks are also due to Prof. S. Seetharaman and Assoc. Prof. Du Sichen for critically reviewing the manuscript.

REFERENCES

1) L. J. P. Ölund, T. B. Lund and B. H. Hedberg: Proc. 5th Int. Clean Steel Conf., Hungarian Mining and Metallurgical Society, and Institute of Materials, London, (1997), 137.
2) Thore Lund: Private communication, Ovako Steel AB, S-813 82 Hofors, Sweden, March (1999).
3) P. Sjödin, P. Jönsson, M. Andreasson and A. Winqvist: *Scand J. Met.*, **26** (1997), 41.
4) R. Nilsson, D. Sichen and S. Seetharaman: Proc. Scaninject VII, MEFOS, Luleå, (1995), 149.
5) M. M. Nzotta, D. Sichen and S. Seetharaman: *ISIJ Int.*, **38** (1998), 1170.
6) M. M. Nzotta, D. Sichen and S. Seetharaman: A Study of the Sulphide Capacities of Iron-oxide Containing Slags, *Met. Trans. B.*, in press.
7) M. M. Nzotta, P. Jönsson and S. Seetharaman: A Study of Sulphide Capacities of Steelmaking Slags, to be published.
8) F. D. Richardson: Physical Chemistry of Melts in Metallurgy, Academic Press, London, (1974), 291.
9) C. J. B. Fincham and F. D. Richardson: *Proc. R. Soc. A*, **A223** (1954), 40.
10) M. R. Kalyanram, T. B. Macfarlane and H. B. Bell: *J. Iron Steel Inst.*, **195** (1960), 58.
11) E. T. Turkdogan: Fundamentals of Steelmaking, The Institute of Materials, London, (1996), 140.
12) D. J. Sosinsky and I. D. Sommerville: *Met. Trans. B*, **17B** (1986), 331.
13) R. W. Young, J. A. Duffy, G. J. Hassall and Z. Xu: *Ironmaking Steelmaking*, **19** (1992), 201.
14) J. A. Duffy and M.D. Ingham: *J. Non-Cryst. Solids*, **21** (1976), 373.
15) R. G. Reddy and M. Blander: *Metall. Trans. B*, **18B** (1987), 591.
16) R. G. Reddy and M. Blander: *Metall. Trans. B*, **20B** (1989), 591.
17) A. Pelton, G. Eriksson and A. Romereo-Senarro: *Metall. Trans. B*, **24B** (1993), 817.
18) H. Gaye and J. Welfringer: Proc. 2nd Int. Symp. on Molten Slags and Fluxes, Met. Soc. AIME, Warrendale, (1984), 357.
19) H. Gaye, P. V. Riboud and J. Welfringer: 3rd Conf. On Molten Slags and Fluxes, The Inst. of Metals, London, (1988), 259.
20) M. G. Frohberg and M. I. Kapoor: *Stahl Eisen*, **19** (1901), 1024.
21) H. Gaye, J. Lehmann, T. Matsumiya and W. Yamada: 4th Int. Conf. On Molten Slags and Fluxes, ISIJ, Tokyo, (1992), 103.
22) M. Temkin: *Acta. Phys. Chim. URSS*, **20** (1945), 411.
23) M. Görnerup: Studies of Slag Metallurgy in Stainless Steelmaking, Doctoral Thesis, Dept. of Metallurgy, KTH, Stockholm, TRITA-TPM 53, (1997), 24.
24) T. A. Engh: Principles of Metal Refining, Oxford University Press, Oxford, (1992), 62.
25) P. Hayes: Process Principles in Minerals & Materials Production, Hayes Publishing Co, Brisbane, (1993), 633.
26) H. Ohta and H. Suito: *Metall. Trans. B*, **29B** (1998), 119.
27) J. Björkvall, Du Sichen and S. Seetharaman: Thermodynamic description of Al_2O_3–CaO–MnO and Al_2O_3–Fe_tO–Mn_tO melts—a model approach, Dept. of Metallurgy, KTH, TRITA-MET 010, (1998).
28) B. Sundman, B. Jansson and J.-O. Andersson: *CALPHAD*, **9** (1985), 153.
29) F. Reinholdsson, A. Lind, R. Nilsson and P. Jönsson: Proc. 5th Int. Clean Steel Conf., Hungarian Mining and Metallurgical Society, and Institute of Materials, London, (1997), 96.
30) B. Hallberg: Formation of Inclusions in the System MgO–Al_2O_3 during Treatment of Al-deoxidised Steel in MgO-lined Ladles, Licentiate Thesis, Dept. of Metallurgy, KTH, Stockholm, TRITA-TPM 35, (1996).
31) J. Pierard, P. Jönsson, D. Sichen, S. Seetharaman and T. Landin: *Ironmaking Steelmaking*, **25** (1998), 374.
32) M. Göransson: Private communication, Ovako Steel AB, S-813 83 Hofors, Sweden, Feb. (1999).
33) S. Seetharaman and D. Sichen: Emerging Separation Technologies for Metals II, The Minerals, Metals & Materials Society, Warrendale, (1996), 317.
34) S. Pizzini and G. Bianchi: *Chim. Ind.*, **54** (1972), 224.